PHYSICAL REVIEW
LETTERS

VOLUME 85 24 JULY 2000 NUMBER 4

Three Dimensional Diffusion Delay Time Tomography

Shimon Coen*
BWPOMR, 22 Miller Avenue, Suite C, Mill Valley, California 94941
(Received 8 October 1999)

Stable numerical convolution of the diffusion impulse time response with a Gaussian wave packet produces a wave packet whose delay time is governed by an eikonal equation where the diffusivity distribution plays the role of the square of the velocity distribution. Diffusion delay time tomography data can approximately image the diffusivity distribution by solving an inverse problem for the eikonal equation with multiple rays that traverse low diffusivity regions not traversed by earlier related methods, and consequently the resolution in such regions is improved. This is important for medical imaging.

PACS numbers: 03.65.Db

Our goal here is to numerically estimate the three dimensional diffusivity distribution within a bounded volume from diffusion impulse time response tomography data measured on the boundary of this volume. We transform the 3D nonlinear inverse problem of the diffusion equation to an equivalent 3D nonlinear inverse problem of the eikonal equation. The data for the inverse problem of the eikonal equation are obtained from the time of advance (the diffusion delay time) of the intensity peak of a complex valued broad Gaussian wave packet (GWP) which results from the numerical convolution of the measured causal diffusion time impulse response with a related complex valued GWP. This new and stable GWP transform is important because the numerical solution of the 3D inverse problem of the eikonal equation requires much less computer time and random access memory and disk space than the corresponding numerical solution of the nonlinear inverse problems of the diffusion equation or electrical impedance tomography [1]. Our GWP transform is related to a quantum GWP transform that we recently introduced for 3D quantum delay time tomography when phase information is not available [2]. Whereas the use of a complex valued GWP in quantum wave propagation [2] is natural, its use in real valued diffusion processes considered here is not natural and, consequently, it must be considered as novel in addition to being new. This "overlap" produces an important, new, and unexpected result that the complex valued 3D diffusion time response due to a broad complex valued GWP source time function is also a broad complex valued GWP. This fundamental result cannot be obtained by standard earlier manipulations of the diffusion equation, but it requires a novel diffusion application of Born's insight of quantum mechanics that a sufficiently monoenergetic complex valued quantum GWP remains approximately undistorted for a long time and distance. This overlap is important and novel because it produces a new, simple, stable, and practical numerical convolution algorithm for the estimation of the diffusion delay time from partial and noisy measurements of diffusion impulse time response data. We also generalize our GWP transform to apply to 3D compressible fluid flow and electromagnetic induction. The former can be used in ground water hydrology. The later can be used in geophysical imaging and in noninvasive medical imaging of the conductivity distribution of lungs, in sharp contrast to electrical impedance tomography systems [1] which require galvanic contacts to the patient which we eliminate by using electromagnetic induction rather than direct current flow. The new 3D diffusion imaging method presented here improves the resolution and stability of earlier related imaging methods [3–4], especially in white holes regions [5] (corresponding to low diffusivity anomalies), which are not traversed by first arrival time rays due to all the source and the receiver combinations, by the inclusion of arrivals and rays that traverse such regions. This is important for the minimization of erroneous diffusion delay time tomography data interpretations in geophysics, hydrology, and especially in medical imaging. The "blackening" of the

white holes by rays that traverse such regions can be also applied to improve the resolution of first arrival time tomography systems [6]. We should emphasize that the 3D diffusion equation considered here cannot be transformed to the 3D Schrödinger equation treated in [2] because the diffusivity distribution is 3D. One can, however, analytically continue the diffusion time impulse response to an equivalent data corresponding to imaginary time, and then modify the nonlinear inversion algorithm of [2] to apply to such data. This imaginary time transformation is, however, computationally time consuming and numerically unstable when applied to partial and noisy experimental data, in sharp contrast to the simple, stable, and fast numerical convolution operation discussed here.

We consider the following 3D diffusion equation

$$\nabla \cdot D\nabla\psi = \psi_t - \delta(t)\delta[\vec{r} - \vec{r}_s], \tag{1}$$

where $\delta(t)$ is a one dimensional Dirac's delta function of time t, $\delta[\vec{r}]$ is the 3D Dirac's delta function, $\vec{r}$ and $\vec{r}_s$ are position vectors in three dimensions, $\psi = \psi(\vec{r}, \vec{r}_s, t)$ is the 3D diffusion impulse response or equivalently the 3D Green's function, $D = D(\vec{r})$ is the 3D positive diffusivity distribution, and ∇ is the 3D gradient operator. The nonlinear inverse problem to be considered here is the approximate determination of the diffusivity distribution $D(\vec{r})$ within a finite volume V from measurements of the diffusion impulse response $\psi(\vec{r}_R, \vec{r}_s, t)$ over a finite time interval $t_{\min} \le t_l \le t_{\max}$, $l = 1, 2, \ldots, L$ and for sufficient number of source positions $\vec{r}_s$ and receiver positions $\vec{r}_R$ on the boundary Γ of this volume, i.e., $\vec{r}_{R_n}, \vec{r}_{s_m} \in \Gamma$, $n = 1, 2, \ldots, N$, $m = 1, 2, \ldots, M$. We parametrize the unknown 3D diffusivity distribution by P positive constant cubic cells, i.e., $D(\vec{r}) = \sum_{p=1}^{P} D_p \phi_p(\vec{r})$, where $D_p > 0$, $\phi_p(\vec{r}) = 1$ when $\vec{r}$ is within the p cell and $\phi_p(\vec{r}) = 0$ when $\vec{r}$ is not within the p cell. So, our nonlinear inverse problem is to practically estimate the P positive constants $\{D_p\}_{p=1}^{P}$ from the specified L discrete positive time values $\{t_l\}_{l=1}^{L}$ and the specified LMN positive constants $\{\psi(\vec{r}_{R_n}, \vec{r}_{s_m}, t_l)\}_{n,m,l=1}^{N,M,L}$ where MN is sufficiently larger than P. This is discussed next.

We convolve both sides of (1) with the following complex valued GWP:

$$g(t) = (2\pi)^{-1} \exp\{-d^2t^2 + i\omega_0 t\}, \tag{2}$$

where $d > 0$, $\omega_0 > 0$, $d \ll \omega_0$, and $i^2 = -1$. Thus, (1) transforms to

$$\nabla \cdot D\nabla\tilde{\psi} = \tilde{\psi}_t - g(t)\delta[\vec{r} - \vec{r}_s], \tag{3}$$

where $\tilde{\psi}$ is the time convolution of ψ with $g(t)$, i.e., $\tilde{\psi} = \tilde{\psi}(\vec{r}, \vec{r}_s, t) = \int_0^\infty \psi(\vec{r}, \vec{r}_s, \xi) g(t - \xi)\, d\xi$, where $\tilde{\psi}$ is acausal even though ψ is causal because $g(t)$ is acausal. We next transform the time t to frequency ω by the Fourier transform and consequently (3) transforms to

$$\nabla \cdot D\nabla\hat{\tilde{\psi}} = i\omega\hat{\tilde{\psi}} - \hat{g}(\omega)\delta[\vec{r} - \vec{r}_s], \tag{4}$$

where $\hat{\tilde{\psi}}$ is the Fourier transform of $\tilde{\psi}$, i.e., $\hat{\tilde{\psi}} = \hat{\tilde{\psi}}(\vec{r}, \vec{r}_s, \omega) = \int_{-\infty}^{\infty} \tilde{\psi}(\vec{r}, \vec{r}_s, t) e^{-i\omega t} dt$, and $\hat{g}(\omega)$ is the Fourier transform of $g(t)$, i.e., $\hat{g}(\omega) = (\sqrt{2\pi}\, d)^{-1} \times \exp\{-[\omega - \omega_0]^2/[2d^2]\}$.

For sufficiently high ω and ω_0, we approximate $\hat{\tilde{\psi}}$ by

$$\hat{\tilde{\psi}} = A\hat{g}(\omega) \exp\{-\sqrt{i\omega}\,\tau\}, \tag{5}$$

where $A = (4\pi D^{1/2}\tau)^{-1}$, $\sqrt{i\omega} = [1 + i\,\mathrm{sgn}(\omega)]|\omega|^{1/2}/\sqrt{2}$, $\mathrm{sgn}(\omega) = 1$ if $\omega > 0$, $\mathrm{sgn}(\omega) = -1$ if $\omega < 0$, $\mathrm{sgn}(\omega) = 0$ if $\omega = 0$, and $\tau = \tau(\vec{r}, \vec{r}_s)$ satisfies the 3D eikonal equation

$$|\nabla\tau(\vec{r}, \vec{r}_s)|^2 = 1/D(\vec{r}) \tag{6}$$

such that $\tau(\vec{r}, \vec{r}_s) \to |\vec{r} - \vec{r}_s|/D^{1/2}(\vec{r})$ as $|\vec{r} - \vec{r}_s| \to 0$. We now apply the inverse Fourier transform to both sides of (5), and this results in

$$\tilde{\psi} = B \int_{-\infty}^{\infty} \hat{g}(\omega) e^{-\sqrt{i\omega}\tau + i\omega t} d\omega\,, \tag{7}$$

where $B = A/[2\pi]$. The "sharply-peaked" Gaussian function $\hat{g}(\omega)$, i.e., $d \ll \omega_0$, allows us to adequately approximate $\sqrt{\omega}$ by its first two Taylor's expansion terms about ω_0, and then we can evaluate the resulting standard integral exactly; this results in a complex valued GWP whose intensity is given by

$$|\tilde{\psi}|^2 = B^2 \exp\{-\sqrt{2\omega_0}\,\tau + d^2\tau^2/[8\omega_0]\} \times \exp\{-d^2[t - \tau/\sqrt{8\omega_0}]^2\}. \tag{8}$$

This intensity reaches its maximum value at the group delay time $t = t_g = t_g(\vec{r}, \vec{r}_s)$ given by

$$t_g = \tau/\sqrt{8\omega_0}\,. \tag{9}$$

So, the convolution of the causal diffusion time impulse response with the complex valued acausal GWP (2) produces a related complex valued GWP whose intensity (8) peaks at the group delay time (9) where τ satisfies the eikonal equation (6) and ω_0 is the angular frequency of the original GWP (2). We can estimate τ in a stable algorithm from the time where the intensity (8) reaches its peak value. Then we can approximately estimate the diffusivity distribution within the volume V from $\tau(\vec{r}_R, \vec{r}_s)$ for a sufficient number of source and receiver positions on the surface Γ that bounds this volume, by numerically solving a practical nonlinear 3D inverse problem for the eikonal equation by methods related to first arrival time tomography for classical waves [6]. We emphasize, however, that we use multiple arrival times and rays that can traverse low diffusivity regions (white holes [5]) and, consequently, our imaging method improves the resolution of earlier related methods [3,4] in such regions. Our imaging method can also be applied to other 3D inverse problems [7–10].

We next provide a numerical proof of concept demonstration for our complex valued GWP transform by applying it numerically to numerically simulated 3D diffusion

TABLE I. Numerical estimation of τ from numerically simulated diffusion impulse response for a uniform diffusivity (left column) and a nonuniform diffusivity corresponding to two uniform half spaces in perfect contact (seven right columns). See Fig. 1 for the rays in the nonuniform diffusivity.

Uniform	Periods	$-2,-2$	$-2,-1$	$-2,0$	$0,0$	$2,2$	$2,1$	$2,-2$
7.00	2π	7.19	6.81	5.76	3.68	3.36	3.49	5.52
7.03	3π	7.29	6.84	5.67	3.66	3.38	3.50	5.53
7.07	4π	7.28	6.86	5.65	3.61	3.34	3.51	5.54
7.11	5π	7.26	6.88	5.58	3.61	3.37	3.51	5.61
7.17	6π	7.32	6.91	5.56	3.61	3.38	3.54	5.63
6.80	efa	6.71	6.31	5.41	3.66	3.41	3.44	5.35
6.80	pdtr	6.12	5.92	5.53	3.95	3.58	3.61	5.49
6.80	gofa	6.80	5.99	5.13	3.40	3.40	3.43	5.30
	gosa	6.86	6.87	7.08	6.80	3.94	3.71	
	gota	7.88	7.43					

time impulse response corresponding to a uniform diffusivity distribution and a diffusivity distribution characterized by two uniform half spaces in perfect contact. The second example clearly demonstrates the central feature of our diffusion group delay time tomography data corresponding to constructive and destructive interference of different diffusion group delay paths which are conceptually related to Feynman's interfering paths [11] and the corresponding Keller's interfering geometrical optics and geometrical diffraction rays [12].

In Table I we show numerically estimated values of τ using our GWP transform for a uniform diffusivity distribution $D = 1$ on the left column and for two uniform half spaces in perfect contact with $D = 1$ for $z < 0$ and $D = 4$ for $z > 0$, where $z = 0$ corresponds to the interface location. The radial distance between the source position and the receiver position is 6.80, $(-2,-1)$ corresponds to source height of 2.0 above the interface and receiver height of 1.0 above the interface, $(2,1)$ corresponds to source height of 2.0 below the interface and receiver height of 1.0 below the interface, etc. The first five entries on the second column from the left show the number of cycles within the time interval $t_{\max} - t_{\min}$, i.e., $\omega_0 = 2\pi/T$, where $T = (t_{\max} - t_{\min})/\text{cycles}$. "gofa", "gosa", and "gota" correspond to geometrical optics first, second, and third arrival time, respectively. "efa" corresponds to the estimated first arrival time from the diffusion impulse response by a robust nonlinear estimation algorithm which fits an effective medium to the measured data [10]. "pdtr" corresponds to the estimated value of τ from the peak of the diffusion impulse response, i.e., $\tau = \sqrt{6t_{\text{peak}}}$, where t_{peak} is the time where the diffusion impulse response reaches its maximum value [10].

Table I shows that our estimated values of τ for the nonuniform diffusivity are approximately related to a weighted average of the corresponding multiple geometrical optics arrivals where the weights are inversely proportional to the difference in their time of arrival relative to the first arrival time. This characteristic can be used to explain our estimated values when the source and receiver are located in the lower diffusivity region where the separation time of the three or two geometrical optics arrivals is "small," and also when the source and receiver are located in the higher diffusivity region or on the interface, where the separation time between the two geometrical optics arrivals is "large" or "infinite" for a single geometrical optics arrival. The most important point to notice here is that our estimated values of τ depend not only on the first arrival time but also on later arrival times so that rays corresponding to these later arrival times are included, in sharp contrast to [3,4] where only first arrival time rays are used. In Fig. 1 we show two geometrical optics rays and a single diffracted ray corresponding to the fourth column of Table I $(-2,-1)$, two geometrical optics rays corresponding to the eighth column of Table I (2,1), and a single geometrical optics ray corresponding to the ninth column of Table I $(2,-2)$. It should be noted that (5) can be generalized to multiple geometrical optics arrivals and multiple diffracted arrivals weighted by their amplitudes and then (8) consists of constructive and destructive interferences that peak at $t = t_g$, which is computationally related to the center frequency ω_0 of our GWP and τ_k, a_k, $k = 1,2,\ldots,\kappa$, where τ_k and a_k are the arrival times and their corresponding amplitudes.

Figure 2 contains 3 panels: top, middle, and bottom. The top panel shows equally angularly spaced "emanating" rays from a single 3D point source on the left and "scattered" by a low diffusivity anomaly. There are two sets

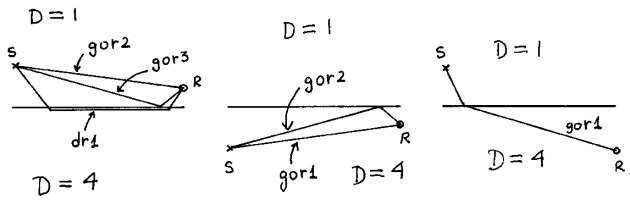

FIG. 1. Sketch of the geometrical optics and geometrical diffraction rays in a discontinuous diffusivity.

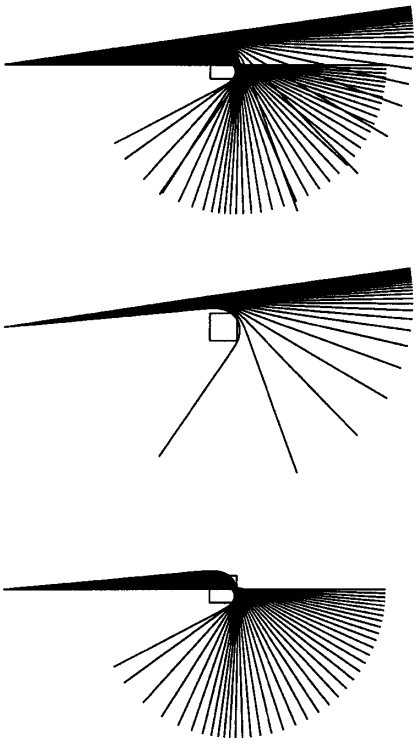

FIG. 2. Rays in the presence of low diffusivity anomaly.

of ray paths. Those that "travel" around the anomaly are shown in the middle panel and those that "travel" through the anomaly are shown in the bottom panel. The rays through the anomaly "arrive" later than the rays around the anomaly. There are regions where the first arrival rays are less dense than these later arrival rays and, consequently, the later arrivals have higher amplitude than the first arrivals there, within the geometrical optics approximation, and therefore, our estimate of τ in such regions is expected to be influenced more by the late arrivals rather than the first arrivals. We can thus improve the resolution of the constructed diffusivity distribution inside low diffusivity regions (white holes [5] which are not traversed by first arrival time rays), in sharp contrast to diffusion first arrival time tomography data used by earlier related imaging methods [3,4], which cannot "sense" such regions [5,10] and lead to erroneous interpretations.

We next generalize our diffusion group delay time tomography to apply to compressible fluid flow and electromagnetic induction in three dimensions. The details are given in [10] but here we discuss the "essentials." The time evolution of the pressure of a compressible fluid flow is governed by a nonlinear diffusionlike equation, but the corresponding time evolution of the fluid density $\gamma = \gamma(\vec{r}, \vec{r}_s, t)$ is governed by the linear diffusionlike equation [13], i.e., $\nabla \cdot (\kappa/\mu)\nabla\gamma = f\beta\gamma_t - \theta(t)\delta[\vec{r} - \vec{r}_s]$ where $\theta(t)$ is the Heaviside step function, $\kappa = \kappa(\vec{r})$ is the permeability distribution, $\mu = \mu(\vec{r})$ is the viscosity distribution, $f = f(\vec{r})$ is the porosity distribution, and the compressibility β is assumed to be a constant. The fluid density can be obtained from the measured fluid pressure by a simple nonlinear analytical relationship. If we convolve the diffusionlike equation satisfied by the density with $dg(t)/dt$ where $g(t)$ is the GWP (2), then, the compressible fluid flow group delay time is given by (9), where τ satisfies the eikonal equation (6) with $D(\vec{r}) = \kappa(\vec{r})/[\beta\mu(\vec{r})f(\vec{r})]$.

Electromagnetic induction is governed by Maxwell's equations where the displacement currents are negligible compared to the conduction currents. The electric field $\vec{E} = \vec{E}(\vec{r}, \vec{r}_s, t)$ for a unit current step time function magnetic dipole source at $\vec{r} = \vec{r}_s$ in the $\hat{z}$ direction satisfies the equation $\nabla \times \nabla \times \vec{E} = -\mu_0\sigma\vec{E} - \mu_0\delta(t)\delta[\vec{r} - \vec{r}_s]\hat{z}$ and away from the source position, $\nabla \cdot \sigma\vec{E} = 0$, where μ_0 is the permeability of free space and $\sigma = \sigma(\vec{r})$ is the conductivity distribution. We convolve the electric field with the complex GWP (2) and then we transform the time t to frequency ω by the Fourier transform. We use the vector equivalent of (5), i.e., $\hat{\vec{E}} = \vec{A}\hat{g}(\omega)\exp\{-\sqrt{i\omega}\,\tau\}$, and this results for sufficiently high ω and ω_0, $\nabla\tau \times \nabla\tau \times \vec{A} = -\mu_0\sigma\vec{A}$, which can be manipulated vectorially to $(\nabla\tau \cdot \vec{A})\nabla\tau - (\nabla\tau \cdot \nabla\tau)\vec{A} = -\mu_0\sigma\vec{A}$, where the first term is negligible for large ω because $\nabla\tau \cdot \vec{A} = \vec{A} \cdot \nabla\sigma/[\sigma\sqrt{i\omega}]$ for $\vec{r} \neq \vec{r}_s$ and, consequently, the electromagnetic induction group delay time is given by (9) where τ satisfies the eikonal equation (6) with $D(\vec{r}) = [\mu_0\sigma(\vec{r})]^{-1}$. Similar results are obtained for the magnetic field [10]. In [3] the phase of the electric field at a fixed and "sufficiently" low frequency (such that the phase is less than 2π) is approximately related to the first arrival time of an "equivalent" wave problem. In [4] the term $[\nabla \times \vec{H} - \vec{J}] \times \nabla \log\sigma$ is neglected so that the magnetic field satisfies a diffusion equation which is transformed to an "equivalent" classical wave equation by an analytical continuation [14] which requires the numerical solution of an ill posed Fredholm integral equation of the first kind for each source and receiver combination. The conductivity distribution is obtained from the transformed data by solving a first arrival time tomography problem. Consequently, neither [3] nor [4] can distinguish between localized "high" conductivity anomalies and "very high" conductivity anomalies which correspond to white holes [5], and therefore the resolution of their constructed approximation to the conductivity distribution is expected to be poor or zero in such regions [5,10], in sharp contrast to the imaging method presented here, which improves the resolution in white hole regions, by the inclusion of late arrival rays that traverse such regions. This resolution improvement is important for the minimization of erroneous data interpretations especially in medical imaging. The numerical convolution operation can be avoided if the GWP is the input source time function when the data are recorded [10].

It is a pleasure to acknowledge useful discussions with Dr. George Basbas and Dr. Daniel M. Beal.

*Email address: optics13@yahoo.com

[1] Y. Kim *et al.,* J. Microwave Power **18**, 245 (1983); D. C. Barber and B. H. Brown, J. Phys. E **17**, 723 (1984); A. Wexler *et al.,* Appl. Opt. **24**, 3985 (1985); B. H. Brown and A. D. Seagar, Clin. Phys. Physiol. Meas. Suppl. A **8**, 91 (1987); J. C. Newell *et al.,* IEEE Trans. Biomed. Eng. **35**, 823 (1988); D. C. Barber, Med. Phys. **16**, 162 (1989); K. S. Chang *et al.,* IEEE Trans. Biomed. Eng. **37**, 60 (1990); J. G. Berryman and R. V. Kohn, Phys. Rev. Lett. **65**, 325 (1990); J. Zhang *et al.,* Geophysics **60**, 1313 (1995); A. Ramirez *et al.,* J. Environ. Eng. Geophys. **1**, 189 (1996).

[2] S. Coen, Phys. Rev. Lett. **83**, 2494 (1999).

[3] G. Nekut, Geophysics **59**, 371 (1994).

[4] K. H. Lee and G. Xie, Geophysics **58**, 780 (1993); U.S. Patent No. 5,373,443 (1994); U.S. Cl. 364/420, 324/338; International Cl. G01V 3/08, G01V 3/18.

[5] S. Coen, Phys. Rev. Lett. **73**, 3219 (1994).

[6] P. Bois *et al.,* Geophysics **57**, 471 (1972); C. G. McKinnon and R. H. T. Bates, Ultrason. Imaging **2**, 49 (1980); J. G. Berryman, Phys. Rev. Lett. **62**, 2953 (1989).

[7] M. Cheney, J. Math. Phys. **25**, 2988 (1984); B. DeFacio and J. H. Rose, Phys. Rev. A **31**, 897 (1985); R. G. Newton, Phys. Rev. A **31**, 3305 (1985).

[8] S. Coen *et al.,* J. Math. Phys. **25**, 1857 (1984).

[9] J. Sajeev *et al.,* J. Biomed. Opt. **1**, 180 (1996).

[10] S. Coen, "3D Multiphysics Digital Imaging from Partial and Noisy Nonlinear Tomography Data" (to be published).

[11] R. P. Feynman, Rev. Mod. Phys. **20**, 367 (1948).

[12] J. B. Keller, J. Appl. Phys. **28**, 426 (1957); Proc. Symp. Appl. Math. **8**, 27 (1958); J. Opt. Soc. **52**, 116 (1962).

[13] M. Muskat and H. G. Botset, Physics **1**, 27 (1931); M. Muskat, Physics **5**, 71 (1934); H. D'Arcy, *Les Fontaines Publiques de la Ville de Dijon* (Victor Dalmont, Paris, 1856).

[14] L. R. Bragg and J. W. Dettman, Bull. Am. Math. Soc. **74**, 375 (1968); SIAM J. Appl. Math. **16**, 459 (1968).